Materials Research Proceedings **26** (2023) 443-448 https://doi.org/10.21741/9781644902431-72

# Identification of normal modes of a set of strongly nonlinear springs

Francesco Latini[1, a *], Jacopo Brunetti[2, b], Walter D'Ambrogio[2, c], and Annalisa Fregolent[1, d]

[1]Dipartimento di Ingegneria Meccanica e Aerospaziale, Università di Roma "La Sapienza", Rome, Italy

[2]Dipartimento di Ingegneria Industriale e dell'Informazione e di Economia, Università dell'Aquila, L'Aquila, Italy

[a]francesco.latini@uniroma1.it, [b]jacopo.brunetti@univaq.it, [c]walter.dambrogio@univaq.it, [d]annalisa.fregolent@uniroma1.it

**Keywords:** Nonlinear Identification, Nonlinear Normal Modes, Nonlinear Time-Series Analysis

**Abstract.** The dynamics of connecting elements should be identified to evaluate their effects on the assemblies where they are employed. In general, a linear analysis is sufficient to determine their dynamics. However, in some cases, their responses depend on the amplitude and frequency of the excitation, thus nonlinear analyses must be carried out. Following a modal approach, Nonlinear Normal Modes (NNMs) can be used. The aim of this work is to identify the NNMs of a set of nonlinear connecting elements properly designed to be considered as strongly nonlinear springs. These elements have been manufactured and tested to measure some of their NNMs. The time series of the oscillation on some points is recorded using a laser vibrometer for different amplitude and frequencies of excitation. Then, the Virtual Point Transformation (VPT) is used to reduce the obtained data on the two physical points through which the spring is connected to other subsystems. The procedure is repeated for each NNM and the modal basis of each element is expressed as function of the level of excitation.

## Introduction

In the last decades the dynamic characterization of joints has become of fundamental importance [1]. Many works have been done to address the problem of bolted joints and lap joints to evaluate their effect in the dynamics of coupled systems. On the other hand, nonlinearities are employed in energy-harvesting applications [2] and in dynamic vibration absorbers [3]. Different studies are focused on the effects that nonlinear connections produce on coupled assemblies. In general, nonlinearities arise when the stiffness and damping properties of the connection depend on some parameters, like the exchanged force or the relative motion between the connected parts. Those dependencies are usually represented using nonlinear laws to approximate the dynamic behavior of the connection. However, in some cases those laws might not represent properly the dynamic behavior of the joint, thus providing misleading results. In those cases, an experimental characterization is the only way to correctly estimate the nonlinear behavior of the connection.

The aim of this work is to characterize the dynamic behavior of a nonlinear element that can be coupled to any subsystem such that it can be regarded as a localized source of nonlinear phenomena. The connecting element considered in this work is suitably designed to exhibit a strong nonlinear behavior. It is derived from the one used in [4] but some adjustments in the design are performed to make it more robust and allow to couple/decouple it to/from the connected parts without affecting its dynamic behavior. Two connecting elements are assembled and tested, following the same procedure described in [5]. They are going to be used as nonlinear connecting elements to couple two beams and obtain an assembly like the one described in [4].

Materials Research Proceedings **26** (2023) 443-448 https://doi.org/10.21741/9781644902431-72

**Description of the Nonlinear Connecting Element**

In the current Section, the new design for the Nonlinear Connecting Element (NLCE) is presented. The connecting element is similar to the one described in [4]. However, some design aspects are improved to make the element more robust and ensure that the junction with other subsystems is localized. Fig. 1 shows the drawings of the NLCE and its 3D model.

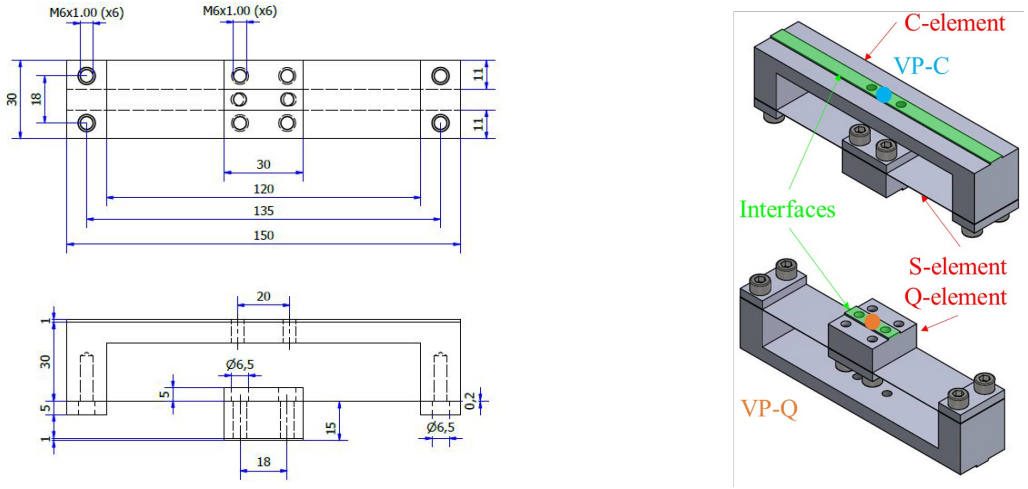


a) Design of the NLCE b) 3D model of the NLCE

*Fig. 1– Design of the NLCE; the dimensions are expressed in millimeters*

It is composed of three main parts: a C shaped element and a block element (referred as C-element and Q-element hereinafter, respectively) connected through a 0.2 mm thick spring-steel sheet (referred as S-element). During the assembly a thermal cycle has been introduced to guarantee a pre-tensile stress on the S-element to avoid buckling phenomena. Fig. 2 shows the first three modes of vibration of the NLCE obtained by performing a linear modal analysis on ANSYS. These are modes of interest because there is a large deformation of the S-element that leads to a significant nonlinear behavior of the NLCE.

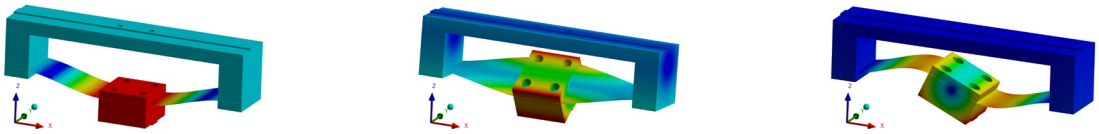

a) First mode b) Second mode c) Third mode

*Fig. 2 – First three modes of vibration of the NLCE*

This design guarantees that once the NLCE is assembled, it can be treated as a unique subsystem, and can be jointed/disjointed to/from other subsystems making it robust and reliable for different tests. As it can be seen from Fig. 2, the three modes are associated with a relative motion between the C- and Q-element due to the deformation of the S-element. For this reason, it is possible to represent the dynamic behavior of the NLCE as the behavior of two masses connected through one longitudinal spring along the z-axis and two rotational springs acting along the x- and y-axis, respectively.

Since the internal deformation of the C- and Q-elements is negligible, a Virtual Point Transformation (VPT) [6] can be applied on their measurement points to obtain the time response on VP-C and VP-Q shown in Fig. 1b. For a given measurement point, the VPT is expressed by:

Materials Research Proceedings **26** (2023) 443-448 https://doi.org/10.21741/9781644902431-72

$$\begin{bmatrix} u_X \\ u_y \\ u_z \end{bmatrix} = \begin{bmatrix} e_{x,X} & e_{x,Y} & e_{x,Z} \\ e_{y,X} & e_{y,Y} & e_{y,Z} \\ e_{z,X} & e_{z,Y} & e_{z,Z} \end{bmatrix} \begin{bmatrix} 1 & 0 & 0 & 0 & r_Z & -r_Y \\ 0 & 1 & 0 & -r_Z & 0 & r_X \\ 0 & 0 & 1 & r_Y & -r_X & 0 \end{bmatrix} \begin{bmatrix} q_X \\ q_Y \\ q_Z \\ q_{\theta X} \\ q_{\theta Y} \\ q_{\theta Z} \end{bmatrix} + \begin{bmatrix} \mu_x \\ \mu_y \\ \mu_z \end{bmatrix} \quad (1)$$

where $\boldsymbol{u}=[u_x,\ u_y\ ,u_z]^T$ is the array containing the displacements in the local frame $(x,y,z)$ of the measurement point accounting for the sensor orientation; $\boldsymbol{q}=[q_X,\ q_Y,\ q_Z,\ q_{\theta X},\ q_{\theta Y},\ q_{\theta Z}]^T$ is the array containing the 6 DoFs of the virtual point in the global frame $(X,Y,Z)$. Moreover, coefficients $(r_X,\ r_Y,\ r_Z)$ represent the distances along the three axes between the measurement point and the virtual point; the matrix of coefficients $e_{i,j}$ with $i=x,y,z$ and $j=X,Y,Z$ represent the transformation matrix between the two frames and the vector of coefficients $\mu_i$ is the residual of displacements associated with the deformation. Note that, only the three DoFs $\boldsymbol{q}=[q_Z,\ q_{\theta X},\ q_{\theta Y}]^T$ are meaningful to characterize the dynamics of the NLCE and only the displacements along the z-axis are measured. Then, the VPT is performed to obtain $\boldsymbol{q_C}$ and $\boldsymbol{q_Q}$. The deformation of the NLCE $\boldsymbol{q_N}$ is:

$$\boldsymbol{q_N} = \boldsymbol{q_C} - \boldsymbol{q_Q} \quad (2)$$

Since the NLCEs are suitably designed to be nonlinear, the resonance frequencies $\omega_N$ vary for increasing levels of the excitation. Moreover, the response along the DoFs $\boldsymbol{q_N}$ to harmonic excitation at a given resonance frequency can be nonlinear and contain super-harmonic components. Thus, each term $q_i(t)$ of $\boldsymbol{q_N}$ can be approximated using a truncated Fourier series:

$$q_i(t) \approx a_{0,i} + \sum_{k=1}^{n} a_{k,i}\cos(k\omega_0 t) + b_{k,i}\sin(k\omega_0 t) \quad (3)$$

This allows to evaluate how the coefficients $a_{0,i}$, $a_{k,i}$ and $b_{k,i}$ vary as the excitation level increases, highlighting the presence of super-harmonic components in the nonlinear modes of both NLCEs.

**Experimental tests**

Two NLCEs are manufactured and assembled following two different thermal cycles such that their dynamics are distinct. Both the NLCEs are tested following the same steps to obtain their linear and nonlinear behavior. In this Section the corresponding test procedures are described. The 1D scanner laser vibrometer Polytec PSV-500 is used to measure the velocity of the grid of points shown in Fig. 3.

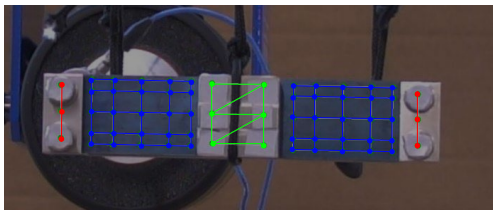

*Fig. 3 – Grid of measurement points of the NLCE: the green points are referred to the Q-element, the red points to the C-element and the blue points to the S-element*

Both the components are tested first using a low amplitude burst random excitation to estimate their linear behavior and then with increasing amplitude harmonic excitation signals to characterize their nonlinear dynamics [5]. In the linear tests, the Polytec software generates the excitation signal for the shaker (2025E Modal shaker, Modal Shop). In the nonlinear tests, instead, the Dewesoft acquisition system is used. The shaker is provided with an impedance head PCB 208 that measures both the force and the acceleration at the excitation point.

Materials Research Proceedings **26** (2023) 443-448 https://doi.org/10.21741/9781644902431-72

**Results of linear tests**

Fig. 4 shows the average spectrum of both NLCEs obtained by performing a linear test. This spectrum allows to localize the natural frequencies of the component in a given frequency range. The different thermal cycle followed for the second NLCE makes its natural frequencies higher than the first NLCE's. The dashed red lines in Fig. 4 highlight the frequencies of the modes of interest identified in the numerical model (Fig. 2) that are considered hereinafter. The resonance frequencies of the three modes are listed in Table 1. Fig. 5 shows the operational deflection shapes performing a Fast Scan analysis by exciting the NLCE with a harmonic force at the frequencies shown in Table 1. The obtained operational deflection shapes comply with the numerical results shown in Fig. 2.


a) First NLCE b) Second NLCE

*Fig. 4 – Average spectra of the two NLCEs*

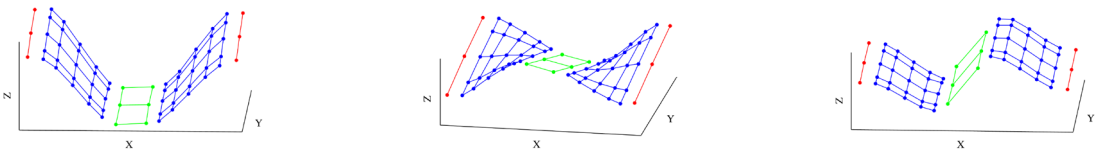

a) First mode b) Second mode c) Third mode

*Fig. 5 – Operational deflection shape of the three modes obtained through Fast Scan analysis*

*Table 1 – Resonance frequencies of three modes of the two NLCEs*

| | Resonance frequency 1st NLCE | Resonance frequency 2nd NLCE | Δ% |
|---|---|---|---|
| First mode | 28.3 Hz | 38.4 Hz | 35.7 |
| Second mode | 53.9 Hz | 57.8 Hz | 7.2 |
| Third mode | 76.1 Hz | 101.8 Hz | 33.8 |

**Results of nonlinear tests**

Once the linear resonance frequencies of the modes of interest are found, it is possible to perform the nonlinear analysis to reconstruct the corresponding Nonlinear Normal Modes (NNMs). The measurement of the NNMs is carried out by setting the amplitude and by adjusting the frequency of the sinusoidal excitation to reach the resonance condition, i.e., when the velocity is in-phase with respect to the excitation force. Once the resonance condition is attained, the velocity of all the points in the grid is recorded and it is integrated to obtain the displacement time series. By setting several excitation levels, it is possible to find the corresponding resonance frequency, thus reconstructing the considered NNM. This procedure is repeated for the three modes of each NLCE, always starting from the low value of amplitude at the identified linear natural frequencies, listed in Table 1.

Materials Research Proceedings **26** (2023) 443-448 https://doi.org/10.21741/9781644902431-72

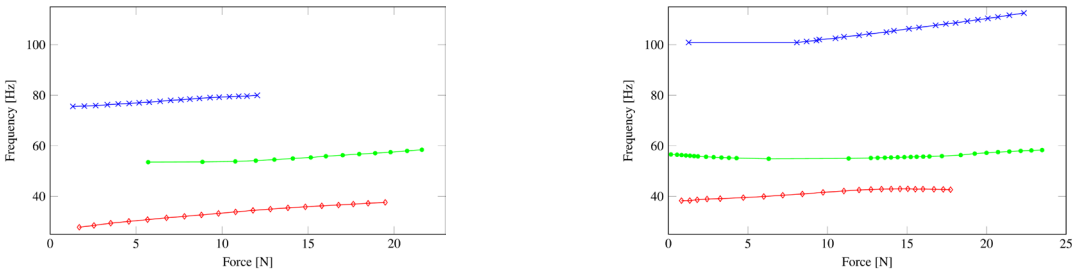


a) First NLCE b) Second NLCE

*Fig. 6 – Frequency-Force Plot of both NLCEs: -◊- first mode; -●- second mode; -x- third mode*

Fig. 6a and 6b show the resonance frequency of the three NNMs versus the excitation force for the first and second NLCE, respectively. Note that the resonance frequencies of the second NLCE are higher than those of the first one, especially for the first and third NNMs. As mentioned before, the internal deformation of the C- and Q-elements is negligible, thus Virtual Points can be introduced to describe their time response. According to the procedure described before, the analysis of the time response of VP-C and VP-Q allows to identify the mode shape of the NNMs associated with the deformation of the S-element. Fig. 7 shows the time responses of VP-C and VP-Q for the first NLCE along the three relevant DoFs ($Z$, $\theta_X$, $\theta_Y$). These displacement signals are obtained applying an excitation force of about 12 N. It is evident that, for each mode, the time response along one DoF is predominant with respect to the others. Nevertheless, the other DoFs have a non-null contribution in the time response, thus they cannot be neglected when estimating the mode shape of the corresponding modes. For example, the time responses along the DoFs $\theta_X$ and $\theta_Y$ of the first mode (Fig. 7 and 7g) show a non-negligible oscillation. Furthermore, it is possible to observe the presence of super-harmonic components. For this reason, the responses can be fitted using a Fourier series according to Eq. (3) truncated at $n=4$. Fig. 8 shows the variation of the Fourier coefficients for increasing levels of excitation on the three DoFs of each mode of the first NLCE. The results highlight that, for each mode, the contribution of the first harmonic of the response along one DoF is predominant with respect to all the other terms. Note that, for the first two modes, there is a non-negligible response for the other DoFs, while for the third mode only the DoF $\theta_Y$ is involved. The Fourier fitting highlights that super-harmonic components are non-negligible, especially in the non-predominant DoFs, e.g. DoF $Z$ for the second mode and DoF $\theta_X$ for the first mode. The results of the second NLCE are similar to those of the first NLCE but they are not shown for the sake of brevity.

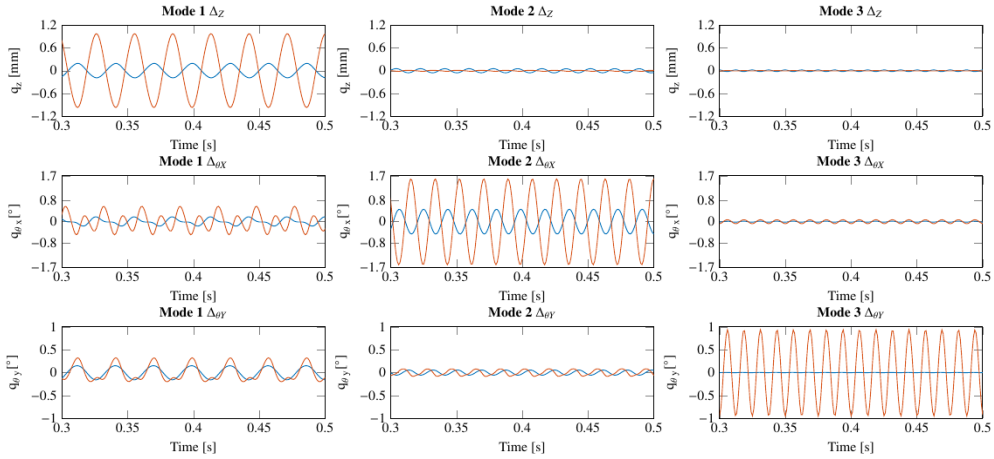


*Fig. 7– Time response of VP-C (-) and VP-Q (-) of the first NLCE for F=12 N.*

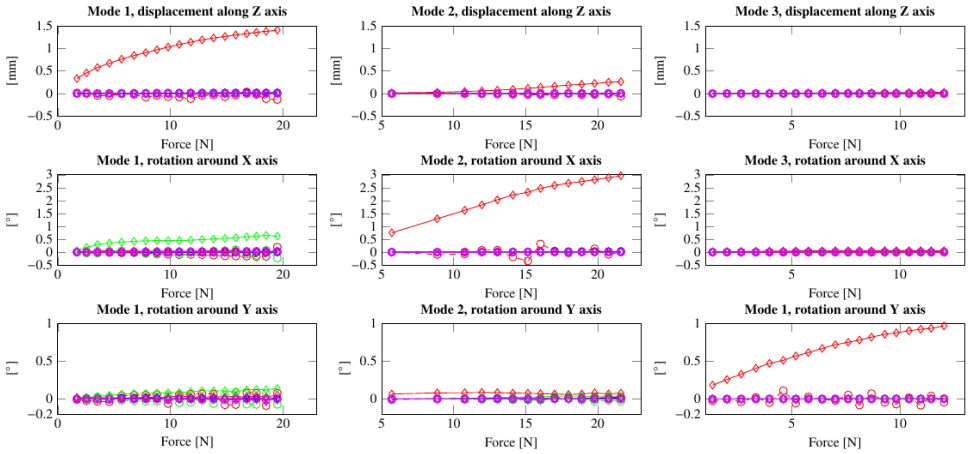


*Fig. 8 – Fourier coefficients of the differential displacements for the three modes of the first NLCE: -$a_0$; -◊ $a_1$; -○- $b_1$; -◊ $a_2$; -○- $b_2$; -◊ $a_3$; -○- $b_3$; -◊ $a_4$; -○- $b_4$.*

**Summary**

In this work, the dynamic behavior of a pair of Nonlinear Connecting Elements is experimentally evaluated. A linear experimental modal analysis is performed and three linear normal modes of interest are identified. Subsequently, nonlinear tests are carried out to identify the corresponding nonlinear normal modes in terms of variation of resonance frequency and mode shape. Since the nonlinearity introduces super-harmonics in the resonant response of the system, their contribution has been evaluated in the nonlinear normal mode identification. The identification procedure carried out on two similar nonlinear connecting elements shows that a different pre-tensioning of the spring-steel sheet significantly affects the nonlinear dynamics of these systems.

**References**

[1] Z. Saeed, S.W.B. Klaassen, C.M. Firrone, T. M. Berruti, D.J. Rixen, Experimental Joint Identification Using System Equivalent Model Mixing in a Bladed-Disk, J. Vib. Acoust. 142 (2020) 1-29. https://doi.org/10.1115/1.4047361

[2] G. Gatti, Optimizing elastic potential energy via geometric nonlinear stiffness, Commun. Nonlinear Sci. Numer. Simul. 103 (2021) 106035. https://doi.org/10.1016/j.cnsns.2021.106035

[3] F.S. Samani, F. Pellicano, Vibration reduction on beams subjected to moving loads using linear and nonlinear dynamic absorbers, J. Sound and Vib. 325 (2009) 742-754. https://doi.org/10.1016/j.jsv.2009.04.011

[4] F. Latini, J. Brunetti, W. D'Ambrogio, M.S. Allen, A. Fregolent, Nonlinear substructuring in the modal domain: numerical validation and experimental verification in presence of localized nonlinearities, Nonlinear Dyn. 104 (2021) 1043-1067. https://doi.org/10.1007/s11071-021-06363-w

[5] F. Latini, J. Brunetti, M. Kwarta, M.S. Allen, W. D'Ambrogio, A. Fregolent, Experimental results of nonlinear structure coupled through nonlinear connecting elements, Proceedings of ISMA 2020, Leuven, Belgium, September 2020, pp. 3011-3022.

[6] M.V. Van der Seijs, D.D. Van den Bosch, D.J. Rixen, D. De Klerk, An improved methodology for the virtual point transformation of measured frequency response functions in dynamic substructuring, Proc. COMPDYN 2013, Kos Island, Greece, June 2013, pp. 4334-4347. https://doi.org/10.7712/120113.4816.C1539